Molecular Neurobiology (2018) 55:8788–8798
https://doi.org/10.1007/s12035-018-1022-z

Delivery of Brain-Derived Neurotrophic Factor by 3D Biocompatible Polymeric Scaffolds for Neural Tissue Engineering and Neuronal Regeneration

T. Limongi[1] · A. Rocchi[2] · F. Cesca[2] · H. Tan[3] · E. Miele[4,5] · A. Giugni[1] · M. Orlando[2,6] · M. Perrone Donnorso[4] · G. Perozziello[7] · Fabio Benfenati[2] · Enzo Di Fabrizio[1]

Received: 14 September 2017 / Accepted: 16 March 2018 / Published online: 29 March 2018

Abstract

Biopolymers are increasingly employed for neuroscience applications as scaffolds to drive and promote neural regrowth, thanks to their ability to mediate the upload and subsequent release of active molecules and drugs. Synthetic degradable polymers are characterized by different responses ranging from tunable distension or shrinkage to total dissolution, depending on the function they are designed for. In this paper we present a biocompatible microfabricated poly-ε-caprolactone (PCL) scaffold for primary neuron growth and maturation that has been optimized for the in vitro controlled release of brain-derived neurotrophic factor (BDNF). We demonstrate that the designed morphology confers to these devices an enhanced drug delivery capability with respect to monolithic unstructured supports. After incubation with BDNF, micropillared PCL devices progressively release the neurotrophin over 21 days in vitro. Moreover, the bioactivity of released BDNF is confirmed using primary neuronal cultures, where it mediates a consistent activation of BDNF signaling cascades, increased synaptic density, and neuronal survival. These results provide the proof-of-principle on the fabrication process of micropatterned PCL devices, which represent a promising therapeutic option to enhance neuronal regeneration after lesion and for neural tissue engineering and prosthetics.

Keywords Microfabrication · Biopolymer · Drug delivery · Primary neurons · BDNF · Neural tissue engineering

T. Limongi and A. Rocchi contributed equally to this work.

F. Benfenati and E. Di Fabrizio are senior authors and corresponders.

Electronic supplementary material The online version of this article (https://doi.org/10.1007/s12035-018-1022-z) contains supplementary material, which is available to authorized users.

✉ Fabio Benfenati
fabio.benfenati@iit.it

✉ Enzo Di Fabrizio
enzo.difabrizio@kaust.edu.sa

[1] SMILEs Lab, Physical Science and Engineering (PSE) and Biological and Environmental Science and Engineering (BESE) Divisions, King Abdullah University of Science and Technology, Thuwal 23955-6900, Kingdom of Saudi Arabia

[2] Center for Synaptic Neuroscience and Technology, Istituto Italiano di Tecnologia, Largo Rosanna Benzi 10, 16132 Genoa, Italy

[3] Analytical Core Lab, King Abdullah University of Science and Technology, Thuwal 23955-6900, Kingdom of Saudi Arabia

[4] Nanostructures Department, Istituto Italiano di Tecnologia, Via Morego 30, 16163 Genoa, Italy

[5] Present address: Centre for BioImaging Sciences, Department of Biological Sciences, National University of Singapore, 14 Science Drive 4, Singapore 117543, Singapore

[6] Present address: Department of Neurophysiology, NeuroCure Excellence Cluster, Charité Universitäts Medizin, Charitéplatz 1, 10117 Berlin, Germany

[7] Laboratory of Nanotechnology BioNEM Department of Experimental and Clinical Medicine, University "Magna Graecia" of Catanzaro, Viale Europa, Catanzaro, Italy

Introduction

Damage to the central nervous system (CNS) under pathological conditions or injury leads to detrimental consequences, which are mainly due to the reduced ability of central neurons to regenerate [1, 2]. To date, the repair of CNS remains one of the major clinical challenges for the field of tissue engineering [3]. A wide range of approaches currently ensure the pharmacological treatment of symptoms, but despite this, there is a critical need of strategies able to overcome disease progression and restore morphology, connections, and functionality of neural circuits [4–7].

Approaches to assist neurogenesis and regeneration include the development of biopolymer-based scaffolds. Biopolymeric devices provide a structural flexible support for cell adhesion and growth and can also provide controlled release of trophic factors [8]. Previous studies have shown the biocompatibility and effectiveness of poly-ε-caprolactone (PCL) substrates for cell culture and tissue engineering applications [9–14]. Regenerative therapies to treat CNS diseases should generally contrast neurodegeneration, as well as target pathological events such as inflammation, ischemia, demyelination, and axonal injury. In this context, neurotrophic factors such as brain-derived neurotrophic factor (BDNF) and cytokines such as interferon-γ successfully supported axonal outgrowth and neuron protection following spinal cord injury [15, 16].

In cell-based therapies for tissue engineering, the ideal scaffold, besides the highest grade of biocompatibility and a compliance mimicking that of brain tissue, should also provide a controlled release of drugs over long or short periods, to decrease inflammation and enhance the regenerative properties of the nervous tissue [17]. Previous studies demonstrated that modified PCL is able to overcome the problem of hydrophobicity [18–20] and that microfeatured scaffolds with a hydrophobic surface promote cell adhesion and differentiation of primary hippocampal neurons [21]. Surface wettability has a significant impact on the attachment, proliferation, migration, and viability of cells and it is intuitive how this aspect might also improve neuronal regrowth in vivo [22]. Therefore, successful implantation of polymeric devices to the nervous system relies on the application of efficiently engineered or microfabricated materials characterized by high biocompatibility and, if required, optimal release efficiency of neurotrophic factors.

BDNF belongs to the family of neurotrophins together with NGF, NT-3, and NT-4 and plays a critical role in neuronal survival, differentiation, and synapse formation during development and throughout adulthood [23]. BDNF binds two receptors: the p75 neurotrophin receptor ($p75^{NTR}$) and the tropomyosin-related kinase B receptor (TRKB). Binding of BDNF to TRKB activates several downstream intracellular pathways involving phospholipase C γ (PLC-γ), phosphatidylinositol 3-kinase (PI3K), and mitogen-activated protein kinase (MAPK)/extracellular signal-related kinase (ERK) [24, 25].

However, BDNF has a limited ability to cross the blood-brain barrier, and therefore, a direct local and prolonged release in the CNS is required to reach an effective and stable concentration and foster neuronal survival and regeneration [26]. Hence, the development of new highly biocompatible scaffolds for neural growth and regeneration that simultaneously allow the local delivery of neurotrophic drugs has attracted increasing attention in the treatment of neurological disorders.

In this study, we focused our interest on the suitability of three-dimensional (3D) hydrophobic micropillared PCL (MP-PCL) devices to store and delivery bioactive molecules to neural cells grown in contact with the scaffold. In particular, we tested the ability of these devices to sustain the 3D growth of neural cells while maintaining and improving viability compared to standard 2D cultures. We established a long-term delivery system for BDNF at physiologically relevant concentrations. The comparison between patterned and flat substrates clearly evidences the enhanced drug delivery capability of the proposed devices. The released BDNF produces a sustained activation of BDNF signaling cascades and increased primary neuron survival. These results provide an effective experimental model based on a micropillared architecture and PCL decoration, where activity, dosage, and release can be effectively monitored for designing novel therapeutic options for neural tissue repair and regeneration.

Materials and Methods

PCL Scaffold Fabrication

The scaffolds were fabricated by hot embossing of PCL pellets (Mn ~ 80,000, pellets, Sigma-Aldrich, #440744, 3 mm in diameter) on microstructured silicon and flat substrates inserted in an aluminum mold (Al-mold; Supp. Fig. 1a) that is composed of a bottom plate, a middle plate, and a top plate fabricated by milling machining (Minitech Machinery). Four silicon substrates were fixed in the Al-mold and centered to the bottom of four cavities having a squared side of 1 cm and a depth of 0.4 mm (Supp. Fig. 1b). The top plate could then be assembled to the rest of the Al-mold by means of alignment pins to recreate the negative shape of the scaffold (Supp. Fig. 1c). Two types of silicon substrates were used for fabricating the PCL scaffolds. Flat silicon substrates cleaved from a polished silicon wafer in squares of 2 cm sides were used for the fabrication of flat PCL (F-PCL) substrates. Microstructured silicon substrates cleaved in squares of the same dimension were used for fabricating the micropillared (MP-PCL) scaffolds. The microstructured silicon substrates were fabricated by deep reactive-ion etching (DRIE) to reproduce a hexagonal matrix of micropillars with a pitch of 30 μm, with nominal diameter

and height of 10 μm. PCL pellets were melted and pressed on top of the silicon substrates in the aluminum mold. The negative tone of the microstructures was replicated on the surface of the PCL scaffold, reproducing the hexagonal matrix of micropillars described above. Finally, the Al-mold conferred to the PCL scaffolds an external cubic shape (1-cm sides, 0.4-mm height).

In detail, three PCL pellets were inserted into each cavity of the assembled mold that was successively placed in a hot pressing machine (P/O/Weber PRESSTRONICS) that allowed controlling the temperature and the force applied to the Al-mold. An initial temperature of 133 °C was set on the hot pressing machine and the Al-mold, packed with three PCL pellets on each cavity, was placed in it. Five minutes after the pellets melted, the temperature was lowered at 68 °C, and the top plate of the Al-mold was pushed towards the PCL pellets contained in the rest of the Al-mold with a force of 3.5 kN and maintained pressed until the system was cooled down to room temperature (RT). On reaching RT, the applied load was released and the Al-mold was removed from the hot pressing machine. Subsequently, the Al-mold was immersed in ice for about 35 min and, when completely cooled down, the scaffolds were detached.

Scaffold Preparation

Single F-PCL and MP-PCL substrates were placed in 24-well culture plates, sterilized by immersion in ethanol (Fluka), washed twice in H_2O, dried in a laminar flow hood, and further sterilized by UV irradiation for 2 h. For BDNF attachment, BDNF (Sigma) was diluted to the final concentration of 300 ng/ml in culture medium, consisting of neurobasal, 2% B27 supplement, 2 mM glutamine, and antibiotics (Life Technologies) and incubated for 14 days in a cell culture incubator (37 °C, 5% CO_2, 95% humidity). For BDNF release studies, the medium was collected and replaced with fresh culture medium at the indicated time points. BDNF levels were determined by an Elisa assay (BDNF Emax® ImmunoAssay System, Promega), according to the manufacturer's protocol. For the culture of primary neurons, substrates were coated by adding Poly-D-Lysine (PDL, Sigma) to a final concentration of 0.1 mg/mL after the exposure to BDNF for 14 days. Substrates were kept in the PDL solution overnight in a cell culture incubator. Before plating the cells, substrates were washed in sterile H_2O. Controls were subjected to the same procedure with the addition of equivalent volumes of the vehicle (H_2O) instead of BDNF.

Preparation of Primary Neurons

All experiments were carried out in accordance with the guidelines established by the European Community Council (Directive 2010/63/EU of 22 September 2010) and were approved by the Italian Ministry of Health. Primary cortical cultures were prepared from wild-type C57 Bl6/J mice (Charles River, Calco, Italy). All efforts were made to minimize suffering and to reduce the number of animals used. Mice were sacrificed by CO_2 inhalation, and 18-day embryos (E18) were removed immediately by cesarean section. Briefly, enzymatically dissociated cortical neurons were plated on PDL (0.1 mg/mL)-coated glass coverslips, F-PCL, or MP-PCL substrates (30,000 cells plated per device). Cultures were incubated at 37 °C, 5% CO_2, 95% humidity in culture medium. Cultures were used at 3, 7, 10, and 21 DIV.

Co-culture Experiments

Primary astrocytes were obtained from cortices of P0 wild-type C57B/L6 mice as previously described [21]. Briefly, cortices were dissected in ice-cold HBSS and incubated in 0.25% trypsin plus 1 mg/mL DNAse for 30 min at 37 °C. Cells were centrifuged, resuspended in culture medium (MEM, 10% horse serum, 33 mM glucose, and antibiotics), and plated onto PDL coated substrates. After 24 h, the medium was replaced and cells were allowed to reach confluence in the following 2 weeks. Cortical neurons were plated onto mature glial cultures that had been starved for 48 h in neuronal culture medium. Co-cultures were grown for 7 days, fixed, and processed for scanning electron microscopy (SEM).

Viability Assay

The viability of neuronal cultures on the various substrates was evaluated as previously described [14]. Briefly, cells were incubated for 3 min at RT in extracellular medium (EM) (NaCl 135 mM, KCl 5.4 mM, $MgCl_2$ 1 mM, $CaCl_2$ 1.8 mM, glucose 10 mM, Hepes 5 mM, pH 7.4) containing 15 μg/mL fluorescein diacetate (FDA), 5 mg/mL propidium iodide (PI), and 3.3 μg/mL Hoechst-33342. After incubation, cells were washed once in EM and immediately imaged. The hardware configuration for the imaging experiments was based on a Nikon Eclipse 80i upright microscope (Nikon Instruments, Prato Calenzano, Italy) equipped with an epifluorescence attachment and a digital camera Nikon DS-Ri1. Cells were imaged sequentially with DAPI (ex350/50, em460/50 to detect Hoechst), EGFP (ex480/30, em 535/40 to detect FDA), and TRITC (ex540/25, em605/55 to detect PI), with a × 10 objective (NIKON Plan Fluor 10X/0.30 WD 16). For each sample, at least five distinct fields of view were acquired. FDA staining was used as a marker of cell-membrane integrity and culture viability. For each field, the ratio of PI-positive (apoptotic) nuclei over the total number of nuclei, identified by Hoechst fluorescence, was calculated. Images were analyzed by using the Image J software (ver. 1.51 k).

RNA Preparation and Real-time PCR Analysis

Total RNA was extracted with Trizol (Invitrogen) according to manufacturer's instructions; purified using RNeasy MinElute Cleanup Kit (Qiagen, Hilden, Germany); and reverse transcribed into cDNA using the SuperScript III First-Strand Synthesis System (Invitrogen). Gene expression was measured by quantitative real-time PCR (qPCR) (CFX96 qPCR Detection System, Biorad, Hercules, CA, USA). Relative gene expression was determined using the 2-ΔΔCT method. Gusb and Hprt1 were used as control housekeeping genes. The list of primers used is provided in Supplementary Table 1.

Protein Extraction and Western Blotting Analysis

Total protein lysates were obtained from cells lysed in radioimmunoprecipitation assay (RIPA) buffer (10 mM Tris-HCl, 1 mM EDTA, 0.5 mM EGTA, 1% Triton X-100, 0.1% sodium deoxycholate, 0.1% sodium dodecyl sulfate (SDS), 140 mM NaCl) containing protease and phosphatase inhibitor cocktails (Roche). The soluble fraction was collected, and protein concentration was determined using a Bicinchoninic Acid (BCA) Protein Assay Kit (Thermo-Fisher Scientific). For Western blotting, protein lysates were denatured at 99 °C in 5X sample buffer (62.5 mM Tris-HCl, pH 6.8, 2% SDS, 25% glycerol, 0.05% bromophenol blue, 5% β-mercaptoethanol, deionized water) and separated by sodium dodecyl sulfate-polyacrylamide gel electrophoresis (SDS-PAGE). The following antibodies were used: phospho-p44/42 MAPK (Erk1/2) (Thr^{202}/Tyr^{204}) (D13.14.4E) (#4370 Cell Signaling); anti-MAP Kinase 1/2 (Erk1/2) (#06182 Millipore); and Gapdh (#2118 Cell Signaling). Signal intensities were quantified by using the ChemiDoc MP Imaging System (GE Healthcare BioSciences,).

Immunofluorescence Staining

Cortical neurons were fixed in phosphate-buffered saline (PBS)/4% paraformaldehyde for 20 min at RT. Cells were permeabilized with 1% Triton X-100 for 5 min, blocked with 2% bovine serum albumin in PBS/Tween 20 0.05% for 30 min at RT, and incubated with primary antibodies in the same buffer for 45 min. The primary antibodies used were mouse monoclonal anti-β-tubulin III (#T2200, Sigma-Aldrich), guinea pig polyclonal anti-vesicular glutamate transporter-1 (VGLUT1, #AB5905, Millipore), and rabbit polyclonal anti-vesicular GABA transporter (VGAT, #131003, Synaptic System). After the primary incubation, neurons were incubated for 45 min with the secondary antibodies in blocking buffer. Fluorescently conjugated secondary antibodies were from Molecular Probes (Thermo-Fisher Scientific; Alexa Fluor 488, #A11029; Alexa Fluor 568, #A11036; Alexa Fluor 647, #A21450). Image acquisitions were performed using a confocal microscope (SP5, Leica Microsystems GmbH, Wetzlar, Germany) at × 63 (1.4 NA) magnification. Z-stacks were acquired every 300 nm; 10 fields/sample. VGLUT and VGAT intensity values were normalized to the relative cell volume calculated on the basis of β-tubulin III labeling. The analysis was conducted using Image J software (ver. 1.51 k). For each set of experiments, all images were acquired using identical exposure settings.

Scanning Electron Microscopy

Biocompatible F-PCL and MP-PCL scaffolds were sputtered with 10 nm of gold using 20 mA as sputter current with a Cressington 208HR 8000 coater. SEM images were acquired through a Quanta 200 (FEI Company) scanning electron microscope operating at 5 kV with 10.5 mm as working distance. Cells grown on the biocompatible devices were fixed and imaged as described in [14].

Porosimetry

Mercury intrusion porosimetry (MIP) (AutoPore IV 9500, Micromeritics GmbH, Moenchengladbach, Germany) was used to measure porosity as described in [27]. Samples were first evacuated to a pressure of 0.5 psia to remove physisorbed gasses from the interior of the sample. Porosimetry measurements were conducted with an equilibration time of 15 s, the pressure was increased incrementally from 0.1 to 60,000 psia, and then decreased gradually back to atmospheric pressure. For each sample, about 0.3 g of material was analyzed by using a 3-cm^3 penetrometer.

Statistical Analysis

Results are presented as means ± sem from at least three independent preparations. Normal distribution of data was assessed using the D'Agostino-Pearson normality test. To compare two normally distributed sample groups, the unpaired Student's *t* test was used. To compare more than two normally distributed sample groups, one-way ANOVA was used, followed by the post hoc Bonferroni's test. A value of $p < 0.05$ was considered significant. Statistical analysis was carried out using the Prism (GraphPad Software V5, Inc.) software.

Results

Fabrication and Characterization of MP-PCL Substrates

Reproducible 1-cm squared F-PCL (Fig. 1a) and MP-PCL (Fig. 1b) scaffolds were realized. SEM imaging documented

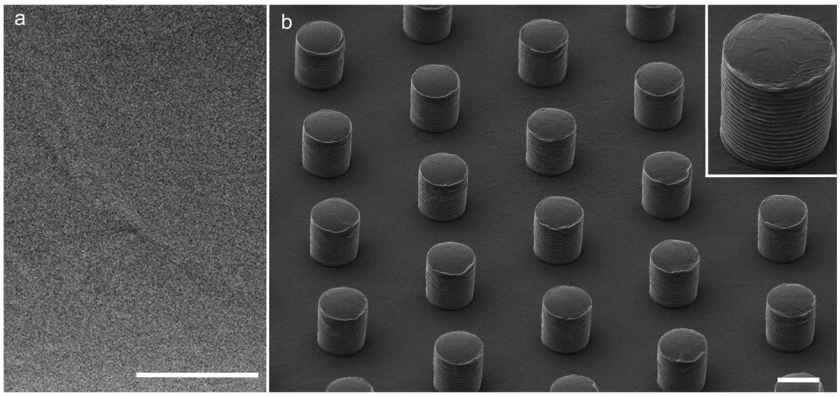

Fig. 1 SEM imaging of the PCL substrates. **a** Flat SEM image of the surface of a F-PCL scaffold and **b** 30°-tilted view of a MP-PCL scaffold with high-resolution details in the inset. Scale bars, 10 μm

the flat surface of the first ones, while microstructured and nanostructured topography was present in the MP scaffolds, characterized by cylindrical pillars of 10 μm in height and in diameter, arranged in a hexagonal lattice with periodicity of 30 μm with nano-thread sidewalls (Fig. 1b, inset).

The spatial arrangement of the pillars on the MP-PCL devices conferred them a much larger surface/volume ratio and a certain grade of porosity associated with the most superficial layers of the scaffold that was not present in the compact and homogeneous surface of the flat device. We quantified this porosity by means of MIP (see "Materials and Methods"), showing that structured samples were characterized by a significantly higher porosity than flat samples ($16.8 \pm 1.3\%$ versus $6.7 \pm 1.2\%$; $p < 0.001$, Student's t test).

MP-PCL Scaffolds Promote Neural Cell Adhesion and Survival

We qualitatively tested cell attachment on MP-PCL scaffolds through SEM imaging and confocal microscopy. MP-PCL devices, thanks to their superficial open scaffold design, assured an effective supply of oxygen and nutrients and a fast elimination of the waste products, and allowed cells to strictly interact with the biomimetic surface. Cultures of cortical neurons (Fig. 2a–c) and astrocytes (Fig. 2d–f) adhered to the MP-PCL surface, forming a well-developed network between contiguous pillars. To further evaluate network formation, primary astrocytes and neurons were processed for confocal fluorescence microscopy using antibodies for actin to visualize the overall cytoskeleton organization. This analysis confirmed the formation of a highly interconnected cell network on the MP-PCL supports (Fig. 2c–f). We also tested the ability of our supports to sustain the growth of co-cultures of primary neurons and astrocytes. As shown by representative SEM images (Fig. 2g–i), astrocytes were able to spread extensively by adhering to the surface of the pillars and by creating a thin carpet to support neuronal survival suspended at the level of the pillars' top, while neurites created an extended and ramified network that firmly embraced the sidewall thread.

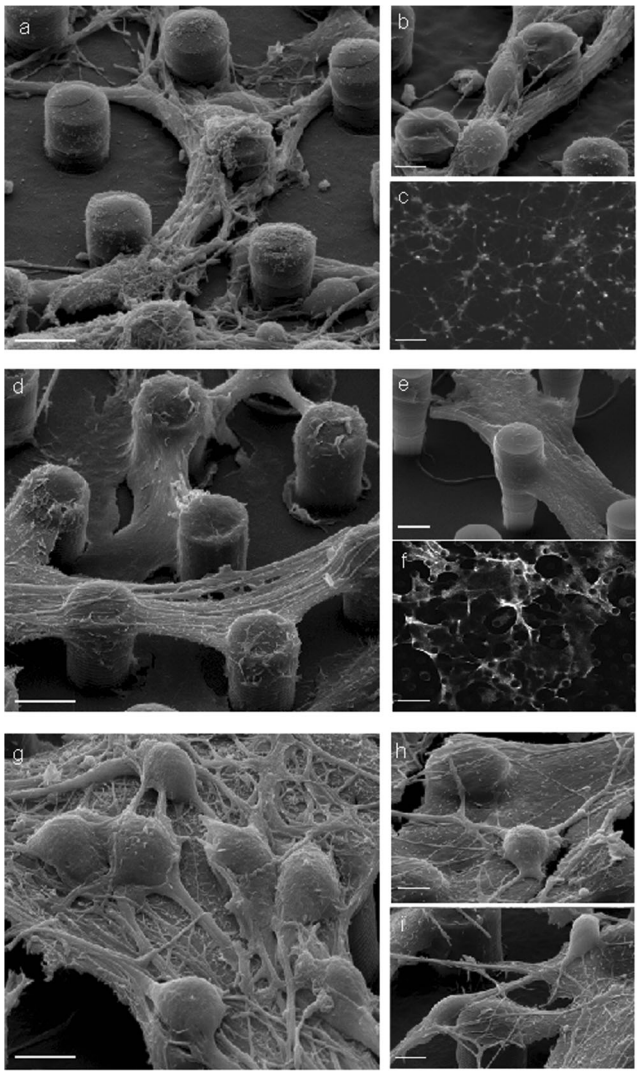

Fig. 2 MP-PCL devices support the growth of primary neuron and astrocyte cultures. Representative SEM images of cortical neurons (**a**, **b**), astrocytes (**d–e**), and neuron/astrocyte co-cultures (**g–i**) grown on MP-PCL substrates. Immunocytochemical characterization of actin expression for astrocyte (**f**) and neuronal (**c**) cultures. Scale bars, 10 μm for SEM images, 50 μm for IF images

After establishing that neuronal cells readily attached to MP-PCL substrates, we compared the viability of primary cortical neuron cultures grown on either F-PCL or MP-PCL devices, as well as onto standard glass coverslips (CTR), at 3, 7, 10, and 21 days in vitro (DIV) (Fig. 3). As expected, a progressive and comparable reduction of neuronal death was observed over time under all culture conditions. However, neurons grown onto MP-PCL supports showed reduced levels of cell death compared to cultures grown on either glass coverslips or F-PCL already at 3 DIV and up to 10 DIV. At later time points (21 DIV), no differences in cell viability were observed, suggesting that MP-PCL substrates promote neuronal survival during the early and critical phases of adhesion and network development.

MP-PCL Substrates Mediate Sustained BDNF Release

One fundamental task in bioengineering is to create biocompatible scaffolds that, beyond passively sustaining cell growth (surface cues), would actively drive cell adhesion and regeneration by releasing chemical cues. In the case of neurons, this would be achieved by obtaining a sustained release of growth factors. We asked whether our MP-PCL devices could serve this purpose and focused on BDNF, one of the most expressed trophic factors in the CNS, which plays a central role in neuronal growth, synaptic plasticity, and regeneration after injury [28, 29]. We incubated MP-PCL scaffolds for 14 days in a solution containing 300 ng/ml BDNF. After the incubation, substrates were washed and BDNF release was measured over a period of 21 days. The distribution of the raw data of BDNF release as a function of time is shown in Fig. 4a. Strikingly, MP-PCL scaffolds were able to release significantly higher amounts of BDNF in the medium than F-PCL devices at all sampled times, an effect that became progressively larger with time. Next, the kinetics of BDNF release was modeled by a bi-exponential function of the form $f(t) = A_0 - A_1$*exp. $(-t/\tau_1) - A_2$*exp. $(-t/\tau_2)$, where A_0 represents the initially available BDNF embedded in the scaffold, τ_1 and τ_2 the time constants of the fast and slow release components, and A_1 and A_2 their respective weights. The kinetic analysis showed that the BDNF release profile could be best described by two distinct release components with clearly different time constants and

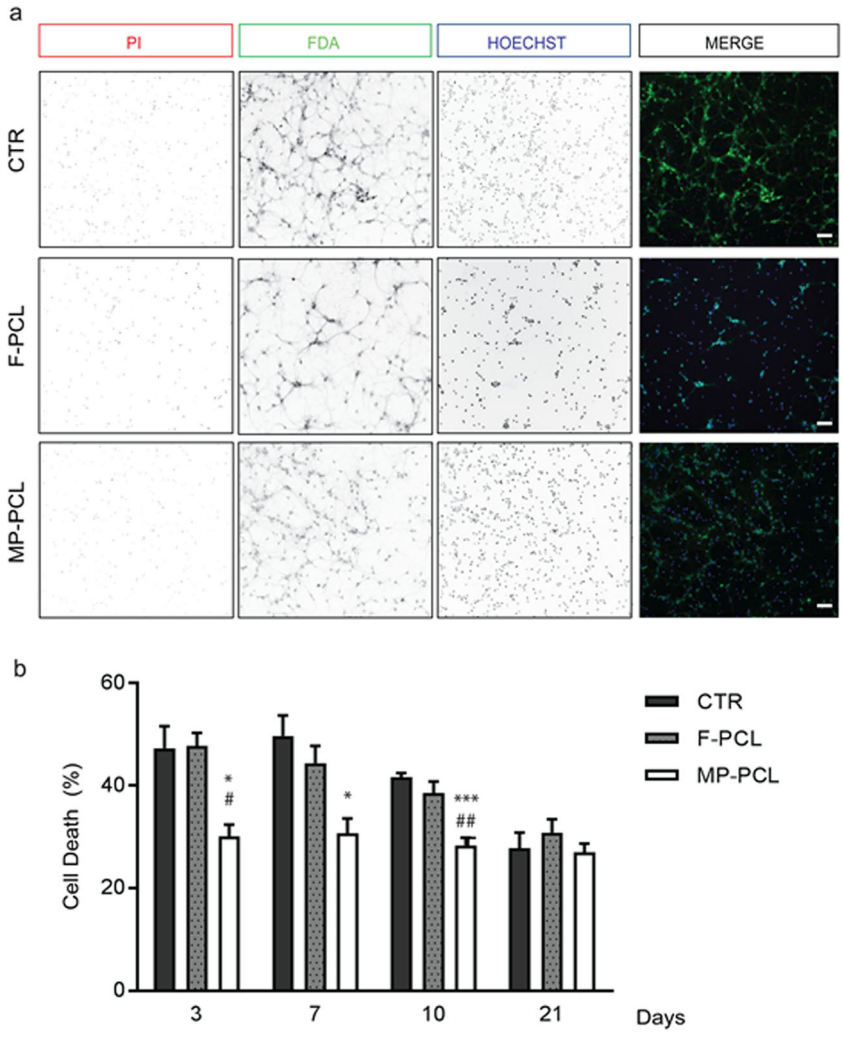

Fig. 3 MP-PCL substrates promote neuronal survival at early stages in vitro. **a** Representative fluorescence microscopy images of 10 DIV neurons plated on standard culture dishes (CTR), F-PCL, or MP-PCL substrates. Neurons were stained with PI (red) for cell death quantification, FDA (green) for cell viability, and Hoechst-33342 (blue) for nuclei visualization (scale bars, 50 μm). **b** Percentages of cell death were calculated as the ratio of PI-positive nuclei on total Hoechst-positive nuclei. Bars are means ± sem from $n = 4$ independent experiments, One-way ANOVA followed by Bonferroni's post hoc test. *$p < 0.05$; ***$p < 0.001$ MP-PCL vs CTR. #$p < 0.05$; ##$p < 0.01$ MP-PCL vs F-PCL

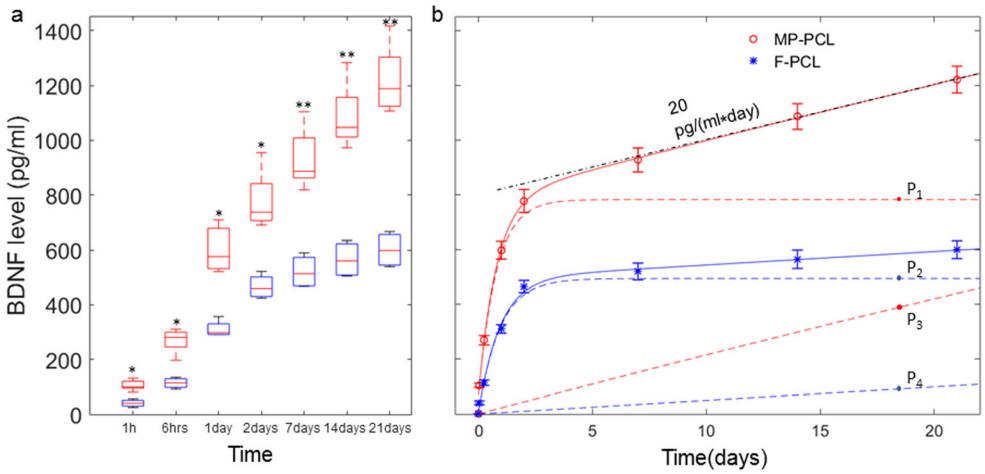

Fig. 4 Cumulative BDNF release from MP-PCL (red boxes) and F-PCL (blue boxes) substrates. **a** Boxplot description of the experimental distributions as a function of time (boxes: first and third quartiles; red line: median; whiskers: 99% coverage). In the inset, the results for the one-tailed *t* test analysis at the 1% significance are reported, assuming an equal population variances. **b** The cumulative BDNF release (means ± sem) as a function of time is described by the sum of two simple exponential curves, drawn as continuous lines. Dashed lines are single exponential components, while a linear regression (dash-dotted black line) depicts the constant long-term release rate of MP-PCL scaffolds

weights ($\tau_1 \sim 19$ h, $\tau_2 \sim 190$ days and $A_1/A_2 = 0.17$ for MP-PCL substrates and $\tau_1 \sim 20$ h, $\tau_2 \sim 1200$ days and $A_1/A_2 = 0.09$ for F-PCL substrates) (Fig. 4b). Both samples show a measurable fast release time constant, τ_1, which is very similar and less than 20 h in both cases. However, the amount of fast released BDNF is higher for MP-PCL substrates (weight ratio: $A_{1-MP}/A_{1-F} \sim 1.6$), consistent with their larger exposed surface. Of particular interest is the comparison of the slow BDNF release component of MP-PCL that has a much higher slope than that of F-PCL, indicating that the different morphology of the substrates affects the long-term release of the growth factor. While F-PCL devices release almost all adsorbed BDNF in the fast process and the residual release is negligible, the MP-PCL samples show a secondary release process that releases BDNF at the constant rate of 20 pg/ml per day with an inferable time constant of 190 days with an overall fivefold larger weight than that of F-PCL (weight ratio: $A_{2-MP}/A_{2-F} \sim 5$) (Fig. 4b). These data suggest that, thanks to its structural, mechanical and physical/chemical properties, our scaffold is characterized by a two-component drug delivery dynamics; a fast early release phase of surface-adsorbed BDNF and a slower release component likely corresponding to the adsorbed BDNF released by the erosion of the permeable MP-PCL structure. Limited to the 20 days of observation time, the MP-PCL structure proves to be capable of releasing more than 30% of the initially available BDNF, resulting in a regular, prolonged release of the growth factor.

BDNF-Functionalized MP-PCL Devices Enhance BDNF Signaling and Neuronal Survival

The long-term biological effects of BDNF are mediated by the activation of intracellular signaling through phosphorylation of a large number of substrates, amongst which Erk1/2 [30]. We therefore asked whether the amount of BDNF released from the PCL devices was sufficient to stimulate BDNF receptors and trigger the activation of BDNF signaling in overlying primary neuronal cultures. We thus monitored Erk1/2 phosphorylation in neurons grown on either F-PCL or MP-PCL substrates exposed to BDNF or vehicle for 14 days. Western blotting analysis with antibodies specific for the dual Thr^{202}/Tyr^{204} phosphorylated Erk1/2 showed that the kinase was significantly more phosphorylated in neurons cultured on BDNF-exposed MP-PCL surfaces compared to control MP-PCL after both 7 and 21 days in culture (Fig. 5a, b). Importantly, we did not detect alterations in the phosphorylation levels of Erk1/2 in cultures grown on F-PCL, both under BDNF and control conditions, suggesting that the superficial topography is crucial to elicit ERK activation.

Because the dual phosphorylation of Erk1/2 activates the kinase and the Erk1/2 cascade positively regulates neuronal survival, we analyzed the impact of BDNF release on the viability of neuronal cultures grown on F-PCL and MP-PCL devices. In agreement with the previous results, neurons grown on MP-PCL surfaces exhibited a lower rate of cell death compared to F-PCL scaffolds at 7 DIV. Notably, the sustained release of BDNF from MP-PCL substrates was able to further and significantly decrease the percentage of cell death to 27%, as compared to the same control substrates at 7 DIV (Fig. 5c). We did not observe any statistically significant difference at 21 DIV, confirming that BDNF signaling affects cell survival predominantly at early stages of neuronal development. On the other hand, the lower and short-lived BDNF release rate from F-PCL substrates did not significantly affect neuronal survival at any time in vitro.

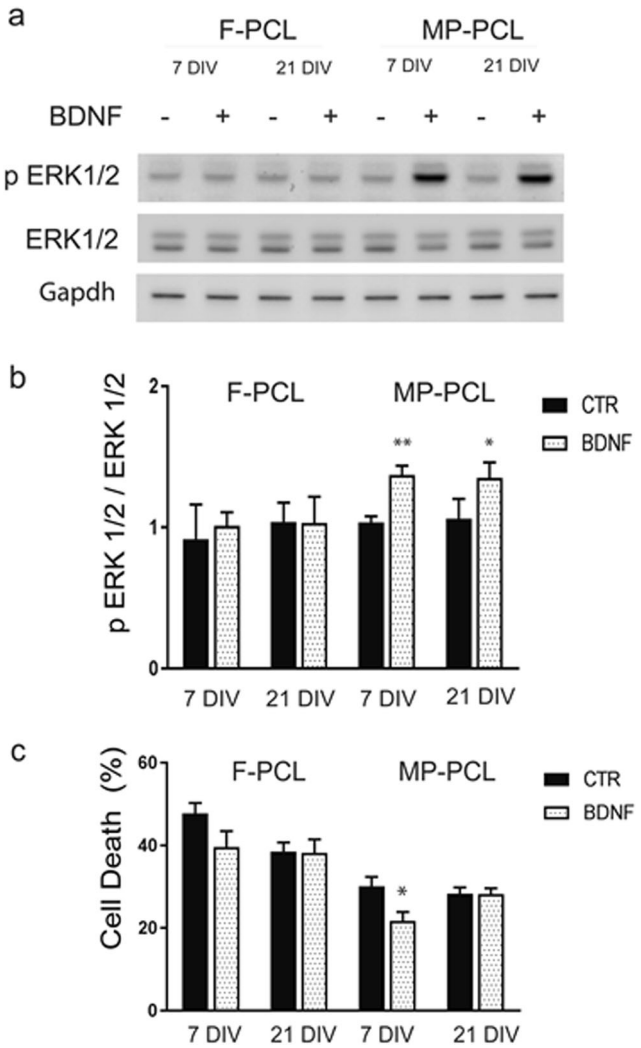

Fig. 5 Enhanced Erk1/2 activation and neuronal survival on BDNF-functionalized MP-PCL devices. **a**, **b** Western blot analysis of phosphorylated and total Erk1/2 in neurons grown on F-PCL and MP-PCL devices that had been treated with vehicle (−) or BDNF (+). Gapdh was used as loading control. A representative experiment is shown (**a**). Immunoreactivity was analyzed and corrected by Gapdh as marker of equal loading (**b**). Data are shown as mean (± sem) stoichiometry ratios between phosphorylated and total Erk1/2 for scaffolds pretreated with either vehicle (black bars) or BDNF (gray bars). $*p < 0.05$, $**p < 0.01$, two-tailed Student's t test ($n = 4$ independent preparations). **c** Cell viability assay performed on neurons grown on F-PCL and MP-PCL devices that had been treated with either vehicle (black bars) or BDNF (dotted bars) and evaluated at 7 and 21 DIV. The percentages of cell death were calculated as the ratio of PI-positive nuclei on total Hoechst-positive nuclei. Data are presented as means ± sem, $*p < 0.05$, two-tailed Student's t test ($n = 3$ independent preparations)

BDNF-Functionalized MP-PCL Devices Enhance the Expression of Synaptic Markers and the Formation of Excitatory and Inhibitory Synapses

To determine whether BDNF release affects synaptic activity, we performed gene expression analysis by real-time PCR on primary cultures grown on F-PCL and MP-PCL substrates. We focused on genes known to be involved in the regulation of synaptic activity and whose expression is regulated by BDNF. Among the various genes, we measured the expression levels of the presynaptic proteins synapsin I (*Syn1*) and synaptotagmin I (*Syt1*) and the postsynaptic glutamate ionotropic receptor AMPA type subunit 1 (*Gria1*), glutamate ionotropic receptor AMPA type subunit 2 (*Gria2*), glutamate ionotropic receptor NMDA type subunit 2A (*Grin2a*), and glutamate ionotropic receptor NMDA type subunit 2B (*Grin2b*) at 7 and 21 DIV.

Consistent with the activation of BDNF signaling demonstrated above, neurons grown on BDNF-exposed MP-PCL devices expressed significantly higher amounts of all synaptic genes at both 7 and 21 DIV, except for *Gria1* and *Grin2b*, whose BDNF-dependent upregulation was significant only at 7 DIV (Fig. 6). On the other hand, neurons developed on F-PCL substrates did not show any BDNF-dependent change in gene expression, except for a slight upregulation of *Syn1* at 7 DIV. Neurons grown on BDNF-treated MP-PCL devices displayed the highest expression of the examined synaptic genes. Moreover, bio-functionalized MP-PCL supports induced a significant increase in the density of both excitatory and inhibitory synapses, confirming the efficacy of the released BDNF in stimulating the formation/maintenance of synaptic connections (Fig. 7). These results suggest BDNF-treated MP-PCL devices are good candidates for enhancing neuronal survival and regeneration, eventually rescuing synaptic connectivity after lesion.

Discussion

The CNS has a poor regenerative ability, which is insufficient to restore the loss of functional neurons upon degenerative pathologies or acute insults. Neuronal survival and activity are largely influenced by the surrounding microenvironment, including the release of growth factors and the complement of extracellular matrix proteins. The main goal of this study was to investigate the efficacy of microfabricated PCL scaffolds to support the formation of neural networks, and to enhance neuronal growth and survival by promoting a sustained delivery of the neurotrophic factor BDNF. We focused on BDNF as it is a crucial factor for several processes of neuronal physiology including neuronal survival, plasticity, and neurogenesis and is therefore considered an attractive therapeutic molecule for neurodegenerative diseases.

The MP-PCL substrates possess multiple properties that make them an ideal scaffold for brain tissue engineering and neural regeneration, namely (i) PCL is highly biocompatible; (ii) it is a conformable and not rigid material that mimics the compliance of nervous tissue; (iii) it provides excellent surface cues for stimulating adhesion

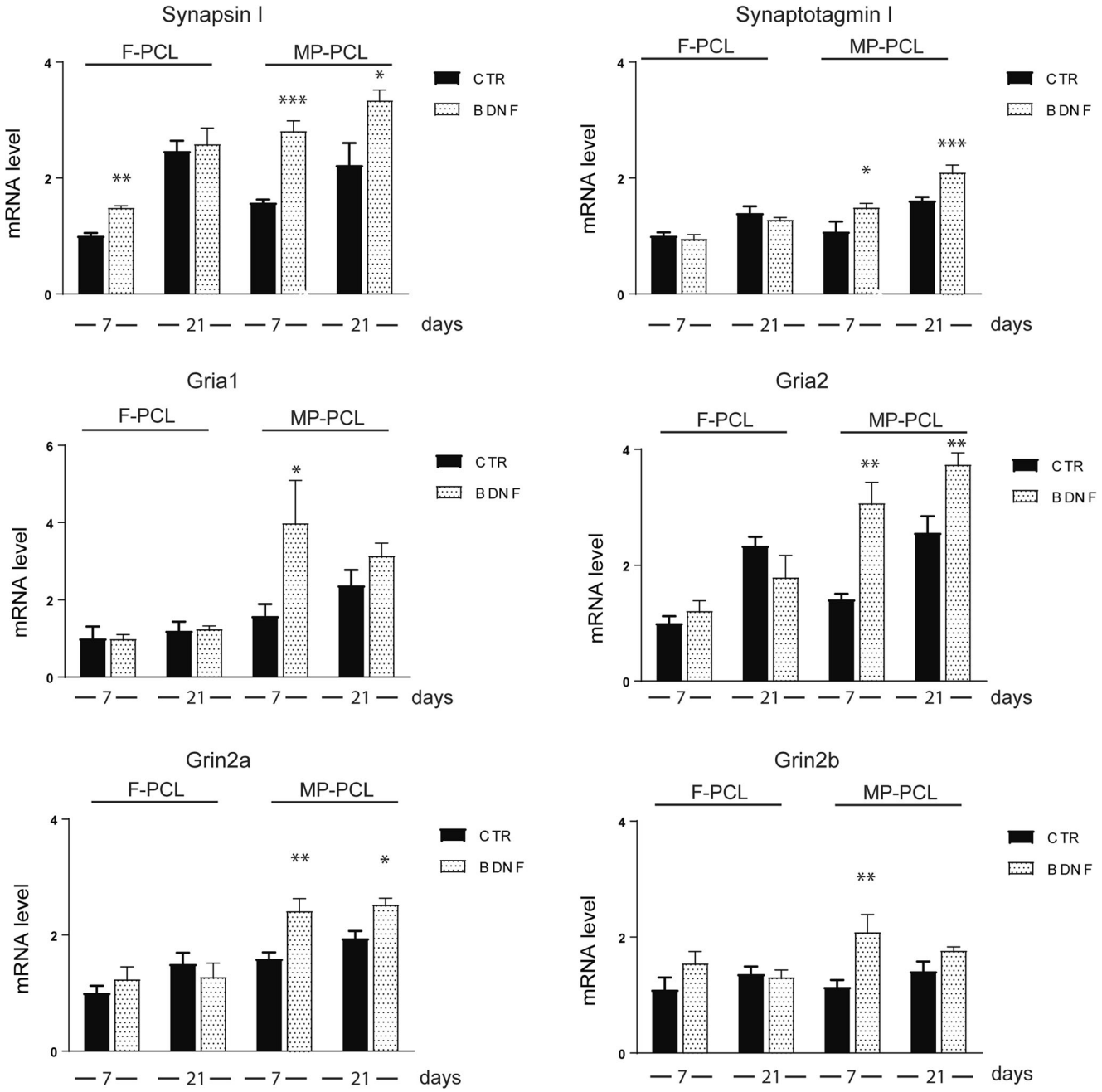

Fig. 6 Synaptic markers regulated by BDNF signaling are increased in neurons cultured on MP-PCL. Syn1, Syt1, Gria1, Gria2, Grin2a, and Grin2b mRNA levels were quantified at 7 and 21 DIV by qRT-PCR in neurons grown on F-PCL and MP-PCL devices treated with vehicle (CTR) or BDNF, as indicated. Gusb and Hprt1 were used as control housekeeping genes. Data are presented as means ± sem (*$p < 0.05$, **$p < 0.01$, two-tailed Student's t test; $n = 4$)

and growth of primary neurons in a 3D arrangement that is more similar to the in vivo condition; (iv) it efficiently absorbs drugs and/or neurotrophic molecules that are slowly and constantly released over time as positive chemical cues for neuronal development and survival; and (v) it can be partially reabsorbed, thus representing an ideal material for tissue regeneration. Our observations showed that MP-PCL substrates are compatible with the growth of both neurons and astrocytes. This is particularly relevant as astrocytes in the brain are the most abundant cellular component and are fundamental for guiding neuronal growth and for exerting protective, trophic, and homeostatic actions on the nearby neurons. Moreover, our viability assays demonstrated that neurons grow and differentiate on MP-PCL devices also in the absence of astrocytes, with a reduced rate of cell death relative to F-PCL substrates. By adsorbing BDNF onto PCL scaffolds, we showed a passive diffusion of the molecule over a

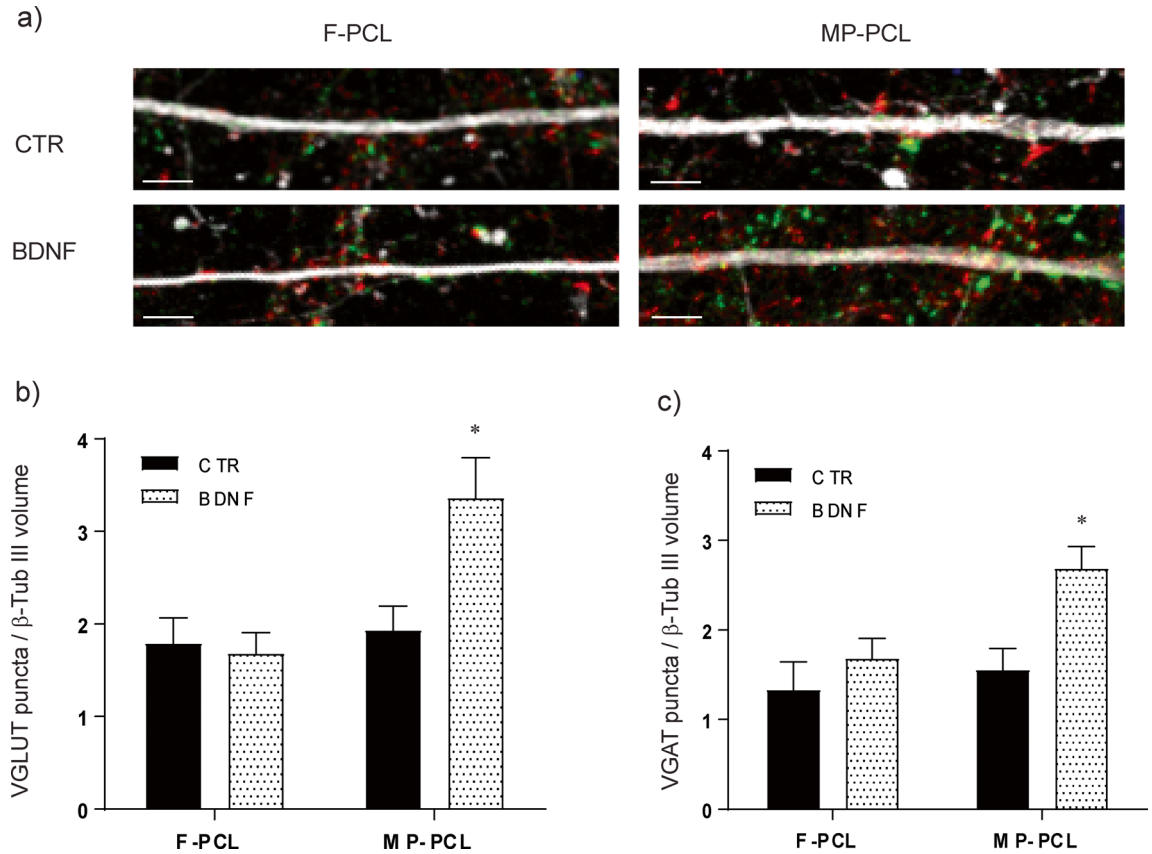

Fig. 7 Density of excitatory and inhibitory synapses in primary cortical neurons cultured on BDNF-functionalized devices for 14 days. (**a**) Representative images of cortical neurons stained for β-III tubulin (gray), VGLUT1 (green), and VGAT (red). Density of VGLUT1-positive excitatory synapses (**b**) and of VGAT-positive inhibitory synapses (**c**) in neurons grown on F-PCL and MP-PCL devices that had been treated with either vehicle (CTR) or BDNF. Scale bars, 10 μm. Data are means ± sem from $n = 3$ independent experiments. Two-way ANOVA followed by Bonferroni's post hoc test. $^*p < 0.05$. CTR MP-PCL vs BDNF MP-PCL

period of 21 days that was the longest time analyzed. Under these conditions, the sustained activation of BDNF signaling was confirmed in primary neurons by the enhanced phosphorylation of Erk 1/2 and increased expression of specific synaptic targets of BDNF. The large proportion of slowly released BDNF from MP-PCL substrates indicates that they can be suitable for long-term neurotrophin release in vivo after surgical implantation.

The efficacy of our biodegradable MP-PCL device lies in the fact that the erosion of the MP-PCL scaffold, thanks to the high surface/volume ratio, occurs much faster than the bulk erosion of the F-PCL surface, thus allowing a more effective drug release. For the development of an efficient drug delivery substrate, material hydrophobicity and porosity have a great influence on the optimal surface morphology and on the choice of proper fabrication methods. Indeed, the presence of microfabricated features on the surface of polymeric degradable scaffolds greatly enhances their drug absorption/delivery capabilities.

In conclusion, the described MP-PCL devices are promising candidates for drug delivery, cochlear and retinal function implants [31], or to assist neural repair after mechanical or pathological injuries [32]. The advancement in the engineering of new polymeric drug delivery systems provides a link between neuroscience, tissue engineering, and drug delivery devices.

Funding Information The work was supported by the King Abdullah University of Science and Technology start-up funding and by research grants from the European Union FP7 "Neuroscaffolds" (grant number 604263 to FB), Compagnia di San Paolo-Italy (to FC).

Compliance with Ethical Standards

Conflict of Interest The authors declare that they have no competing interest.

References

1. Silver J, Miller JH (2004) Regeneration beyond the glial scar. Nat Rev Neurosci 5(2):146–156. https://doi.org/10.1038/nrn1326
2. Fawcett JW, Asher RA (1999) The glial scar and central nervous system repair. Brain Res Bull 49(6):377–391

3. Orive G, Anitua E, Pedraz JL, Emerich DF (2009) Biomaterials for promoting brain protection, repair and regeneration. Nat Rev Neurosci 10(9):682–692. https://doi.org/10.1038/nrn2685
4. Huang L, Wang G (2017) The effects of different factors on the behavior of neural stem cells. Stem Cells Int 2017:9497325. https://doi.org/10.1155/2017/9497325
5. Lancaster MA, Corsini NS, Wolfinger S, Gustafson EH, Phillips AW, Burkard TR, Otani T, Livesey FJ et al (2017) Guided self-organization and cortical plate formation in human brain organoids. Nat Biotechnol 35(7):659–666. https://doi.org/10.1038/nbt.3906
6. Wang LL, Zhang CL (2018) Engineering new neurons: in vivo reprogramming in mammalian brain and spinal cord. Cell Tissue Res 371(1):201–212. https://doi.org/10.1007/s00441-017-2729-2
7. Faustino C, Rijo P, Reis CP (2017) Nanotechnological strategies for nerve growth factor delivery: therapeutic implications in Alzheimer's disease. Pharmacol Res 120:68–87. https://doi.org/10.1016/j.phrs.2017.03.020
8. Tam RY, Fuehrmann T, Mitrousis N, Shoichet MS (2014) Regenerative therapies for central nervous system diseases: a biomaterials approach. Neuropsychopharmacology 39(1):169–188. https://doi.org/10.1038/npp.2013.237
9. Yoshimoto H, Shin YM, Terai H, Vacanti JP (2003) A biodegradable nanofiber scaffold by electrospinning and its potential for bone tissue engineering. Biomaterials 24(12):2077–2082
10. Kim HJ, Lee JH, Im GI (2010) Chondrogenesis using mesenchymal stem cells and PCL scaffolds. J Biomed Mater Res A 92(2):659–666. https://doi.org/10.1002/jbm.a.32414
11. Mathews A, Colombus S, Krishnan VK, Krishnan LK (2012) Vascular tissue construction on poly(epsilon-caprolactone) scaffolds by dynamic endothelial cell seeding: effect of pore size. J Tissue Eng Regen Med 6(6):451–461. https://doi.org/10.1002/term.449
12. Shirian S, Ebrahimi-Barough S, Saberi H, Norouzi-Javidan A, Mousavi SM, Derakhshan MA, Arjmand B, Ai J (2016) Comparison of capability of human bone marrow mesenchymal stem cells and endometrial stem cells to differentiate into motor neurons on electrospun poly(epsilon-caprolactone) scaffold. Mol Neurobiol 53(8):5278–5287. https://doi.org/10.1007/s12035-015-9442-5
13. Limongi T, Miele E, Shalabaeva V, Rocca RL, Schipani R, Malara N, Angelis FD, Giugni A, Fabrizio ED (2015) Development, characterization and cell cultural response of 3D biocompatible micropatterned poly-ε-caprolactone scaffolds designed and fabricated integrating lithography and micromolding fabrication techniques. J Tissue Sci Eng
14. Cesca F, Limongi T, Accardo A, Rocchi A, Orlando M, Shalabaeva V, Di Fabrizio E, Benfenati F (2014) Fabrication of biocompatible free-standing nanopatterned films for primary neuronal cultures. RSC Adv 4(86):45696–45702. https://doi.org/10.1039/C4RA08361J
15. Victorio SC, Havton LA, Oliveira AL (2010) Absence of IFNγ expression induces neuronal degeneration in the spinal cord of adult mice. J Neuroinflammation 7:77. https://doi.org/10.1186/1742-2094-7-77
16. Zhang L, Ma Z, Smith GM, Wen X, Pressman Y, Wood PM, Xu XM (2009) GDNF-enhanced axonal regeneration and myelination following spinal cord injury is mediated by primary effects on neurons. Glia 57(11):1178–1191. https://doi.org/10.1002/glia.20840
17. Liechty WB, Kryscio DR, Slaughter BV, Peppas NA (2010) Polymers for drug delivery systems. Annu Rev Chem Biomol Eng 1:149–173. https://doi.org/10.1146/annurev-chembioeng-073009-100847
18. Dash TK, Konkimalla VB (2012) Polymeric modification and its implication in drug delivery: poly-epsilon-caprolactone (PCL) as a model polymer. Mol Pharm 9(9):2365–2379. https://doi.org/10.1021/mp3001952
19. Sanna V, Siddiqui IA, Sechi M, Mukhtar H (2013) Resveratrol-loaded nanoparticles based on poly(epsilon-caprolactone) and poly(D,L-lactic-co-glycolic acid)-poly(ethylene glycol) blend for prostate cancer treatment. Mol Pharm 10(10):3871–3881. https://doi.org/10.1021/mp400342f
20. Siafaka PI, Barmpalexis P, Lazaridou M, Papageorgiou GZ, Koutris E, Karavas E, Kostoglou M, Bikiaris DN (2015) Controlled release formulations of risperidone antipsychotic drug in novel aliphatic polyester carriers: data analysis and modelling. Eur J Pharm Biopharm 94:473–484. https://doi.org/10.1016/j.ejpb.2015.06.027
21. Limongi T, Cesca F, Gentile F, Marotta R, Ruffilli R, Barberis A, Dal Maschio M, Petrini EM et al (2013) Nanostructured superhydrophobic substrates trigger the development of 3D neuronal networks. Small 9(3):402–412. https://doi.org/10.1002/smll.201201377
22. Limongi T, Pagliari G, Allione P, Candeloro FD (2017) Fabrication and applications of micro/nanostructured devices for tissue engineering. Nano-Micro Letters 9(1)
23. Garraway SM, Huie JR (2016) Spinal plasticity and behavior: BDNF-induced neuromodulation in uninjured and injured spinal cord. Neural Plast 2016:9857201. https://doi.org/10.1155/2016/9857201
24. Cesca F, Yabe A, Spencer-Dene B, Scholz-Starke J, Medrihan L, Maden CH, Gerhardt H, Orriss IR et al (2012) Kidins220/ARMS mediates the integration of the neurotrophin and VEGF pathways in the vascular and nervous systems. Cell Death Differ 19(2):194–208. https://doi.org/10.1038/cdd.2011.141
25. Yoshii A, Constantine-Paton M (2010) Postsynaptic BDNF-TrkB signaling in synapse maturation, plasticity, and disease. Dev Neurobiol 70(5):304–322. https://doi.org/10.1002/dneu.20765
26. Autry AE, Monteggia LM (2012) Brain-derived neurotrophic factor and neuropsychiatric disorders. Pharmacol Rev 64(2):238–258. https://doi.org/10.1124/pr.111.005108
27. Limongi T, Giugni A, Tan H, Bukhari EM, Torre B, Allione M, Marini M, Tirinato L et al (2015) Fabrication, mercury intrusion porosimetry characterization and in vitro qualitative analysis of biocompatibility of various porosities polycaprolactone scaffolds. J Tissue Sci Eng 6. https://doi.org/10.4172/2157-7552.1000159
28. Kelamangalath L, Smith GM (2013) Neurotrophin treatment to promote regeneration after traumatic CNS injury. Front Biol (Beijing) 8(5):486–495. https://doi.org/10.1007/s11515-013-1269-8
29. Wilhelm JC, Xu M, Cucoranu D, Chmielewski S, Holmes T, Lau KS, Bassell GJ, English AW (2012) Cooperative roles of BDNF expression in neurons and Schwann cells are modulated by exercise to facilitate nerve regeneration. J Neurosci 32(14):5002–5009. https://doi.org/10.1523/JNEUROSCI.1411-11.2012
30. Revest JM, Le Roux A, Roullot-Lacarriere V, Kaouane N, Vallee M, Kasanetz F, Rouge-Pont F, Tronche F et al (2014) BDNF-TrkB signaling through Erk1/2 MAPK phosphorylation mediates the enhancement of fear memory induced by glucocorticoids. Mol Psychiatry 19(9):1001–1009. https://doi.org/10.1038/mp.2013.134
31. Chikar JA, Hendricks JL, Richardson-Burns SM, Raphael Y, Pfingst BE, Martin DC (2012) The use of a dual PEDOT and RGD-functionalized alginate hydrogel coating to provide sustained drug delivery and improved cochlear implant function. Biomaterials 33(7):1982–1990. https://doi.org/10.1016/j.biomaterials.2011.11.052
32. Quigley AF, Bulluss KJ, Kyratzis IL, Gilmore K, Mysore T, Schirmer KS, Kennedy EL, O'Shea M et al (2013) Engineering a multimodal nerve conduit for repair of injured peripheral nerve. J Neural Eng 10(1):016008. https://doi.org/10.1088/1741-2560/10/1/016008